# Influence of surface finishing and heat treatments on the corrosion resistance of LPBF-produced Ti-6Al-4V alloy for biomedical applications

M Cabrini, A Carrozza, S Lorenzi, T Pastore, C Testa, D Manfredi, P Fino, F Scenini

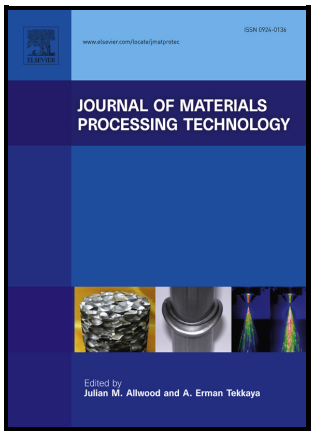


PII: S0924-0136(22)00241-2

DOI: https://doi.org/10.1016/j.jmatprotec.2022.117730

Reference: PROTEC117730

To appear in: *Journal of Materials Processing Tech.*

Received date: 7 June 2022
Revised date: 13 July 2022
Accepted date: 17 July 2022

Please cite this article as: M Cabrini, A Carrozza, S Lorenzi, T Pastore, C Testa, D Manfredi, P Fino and F Scenini, Influence of surface finishing and heat treatments on the corrosion resistance of LPBF-produced Ti-6Al-4V alloy for biomedical applications, *Journal of Materials Processing Tech.*, (2022) doi:https://doi.org/10.1016/j.jmatprotec.2022.117730

# Influence of surface finishing and heat treatments on the corrosion resistance of LPBF-produced Ti-6Al-4V alloy for biomedical applications

**Cabrini M[1,2], Carrozza A[1,2], Lorenzi S[1,2], Pastore T[1,2], Testa C[1,2], Manfredi D[2,3], Fino P[2,3], Scenini F[4]**

[1]*Department of Engineering and Applied Science, University of Bergamo, Dalmine (BG), Italy*

[2]*National Interuniversity Consortium of Materials Science and Technology (INSTM), Firenze, Italy*

[3]*Department of Applied Science and Technology, Politecnico di Torino, Torino, Italy*

[4] *Corrosion and Protection Centre, Materials Performance Centre, Department of Materials, University of Manchester, Manchester, United Kingdom*



## Keywords

Additive manufacturing; Titanium; Ions release; Biocompatibility; Passive current

## Abstract

Additive manufacturing (AM) technologies are gaining increasing attraction for biomedical applications due to the granted customizability and optimal surface topography for osteointegration. Ti-6Al-4V is one of the most promising materials due to its biocompatibility. However, excessive ions release can occur, leading to a relevant immunologic response in the surrounding tissues. Despite the corrosion behavior of the conventionally-manufactured material being well known, it should be assessed for AM-processed components, as the effect of the unique superficial and microstructural features granted by the process is still quite unknown. The aim of this paper is the electrochemical evaluation of the passive current density of the laser powder bed fusion (LPBF)-processed Ti-6Al-4V alloy via potentiostatic tests, carried out at typical in-service potentials for biomedical implants. This parameter is correlated with the ion release rate of the alloy, a fundamental phenomenon to address to prevent possible inflammations caused by the implant. Different manufacturing conditions (surface finishing, heat treatment) and exposure time (0, 60 and 6000 hours) were considered. The importance of performing these measurements over a long period (> 8 months) was demonstrated. In fact, despite the initial current densities being significantly affected by the surface and microstructural differences, the ion release rates converged for long-time exposures. The results also underlined the good corrosion resistance of the material. Poor corrosion performances, alongside with significant current densities development, were observed in the as-built condition. A pickling treatment demonstrated to mitigate such effect without compromising the unique surface finishing granted by the manufacturing

technology.

## 1. Introduction

The Ti-6A1-4V alloy is widely used as a biomaterial for orthopedic applications due to its good compatibility with human tissues, high strength and fatigue resistance (Chen and Thouas, 2015). Nowadays the additive manufacturing (AM) techniques are gaining growing relevance in the field of orthopedic regenerative medicine, specifically for customizable prosthesis production (hip joints, knees), owing to the possibility to create finished components that mimic the anatomical characteristics of the patient, as reported in a multi-field study by Bertol et al. (2010). In addition, AM technologies can be adopted to print metallic implants with controlled porosity and an elastic modulus matching closely that of the native bones, thereby reducing problems related to stress shielding, a critical feature for human implants, according to Kaur et al. (2019). Among these manufacturing techniques, the laser powder bed fusion (LPBF) technology, also referred to as selective laser melting (SLM) or direct metal laser sintering (DMLS), deploys a laser source to selectively melt a metal powder layer by layer, in compliance with a three-dimensional computer-aided design (CAD) model (Frazier, 2014). In a review from Trevisan et al. (2018) , the LPBF process is described as very well consolidated for titanium alloys production. This is also established by other authors, such as Kolli and Devaraj (2018) and Liu and Shin (2018). Recently, Carrozza et al. (2021a) confirmed the industrial interest in AM-produced titanium alloys due to the number of the available materials constantly increasing in the latest years. Furthermore, Liu et al. (2019) reported that the LPBF process typically generates rough surfaces favoring osseointegration, as stated by Kienapfel et al. (1999). This feature is very important, in fact osteoblasts and chondrocytes are sensitive to subtle differences in surface roughness and surface chemistry, according to Boyan et al. (1996). Groessner-Schreiber and Tuan (1992) suggested that porous or rough titanium implant surfaces may act like "natural" substrates, thus favoring microscopic tissue/cell ingrowth and improving clinical implant fixation. In fact, in their work they reported that the synthesis of extracellular matrix and subsequent mineralization were both substantially enhanced in the cultures on rough-textured and porous-coated titanium. In addition, Arabnejad et al. (2016) described how a rough surface can act as an optimal support for osteointegration coatings, like hydroxyapatite.

Both the microstructure and the passive film of the LPBF-produced alloy are significantly different from those present on the alloys obtained via traditional wrought processes. Moreover, these features can be further modified by post-processing heat treatments performed for instance to remove internal stresses. For instance, Yang et al. (2017) investigated the corrosion behavior of the Ti-6Al-4V alloy in a NaCl solution. The specimens were analyzed in the as-built and heat-treated condition, proving the importance of several microstructural features (type of phase, size, etc.) in determining the corrosion resistance of the material. Moreover, the behavior of the protective oxide film was different in the as-built samples, which provided extended cracking phenomena. Additionally, (Pathania et al. (2022) explored several heat treatments on the LPBF-produced Ti-6Al-4V alloy. Thus achieving a wide variety of microstructures (and phases), suggesting a possible significant variability in the corrosion behavior for this material. In fact, post-processing microstructural modification is a key aspect to optimize in order to improve the corrosion resistance. Aufa et al. (2022) highlighted that the corrosion behavior of the LPBF-processed Ti-6Al-4V alloy is mainly related to the formation of α’ martensite on the surface of the implant. Sharma et al. (2020) found in this feature, alongside the emerging pores on the surface, the cause of a general decrease in terms of corrosion resistance with respect to the

convetionally-manufactured material. This behavior is also confirmed by Dai et al. (2016). This is the main reason why a relevant number of works focusing on heat treatments aimed at improving the corrosion resistance of the Ti-6Al-4V alloys are available in the literature (e.g., Pal et al., 2021, Yan et al., 2020).

Several authors, including Fojt et al. (2018) and Longhitano et al. (2018), showed that the nature of the passive film does not influence cell growth but can modify the passive current density. For example, Guo et al. (2017) investigated the antibacterial and anti-corrosion properties of different titanium alloys, concluding that the cell viability was significantly altered only by the composition.

A variation in the passive current density results in a variation the ions release to the surrounding tissue (Okazaki and Gotoh, 2005). Therefore, this phenomenon can be deployed to estimate the ions release rate in surgical implant, as performed by Buchanan et al. (1987). For instance, Cruz et al. (2022) used the evaluation of the current density in Ti-6Al-4V dental implants to investigate innovative passivation processes. The authors stated that this step was fundamental to investigate ionic leakage phenomena, a major risk for patients. In fact, titanium is characterized by a very low thermodynamic equilibrium potential and a strong resistance to corrosion due to its ability to form a electro-insulating, thin and stable passive layer of oxide that protects the substrate from further oxidation. Passivity is a kinetic equilibrium condition between the film dissolution and its re-formation on the metal surface. The re-growth of the passive film involves the oxidation of the base metal. In biological environments, the passive film is modified by short-time and long-time tissue-material interactions. Whilst the physical and chemical phenomena occur instantaneously after the implantation, the long-term situation is more complex to adress, since inflammatory reactions could take minutes to years to manifest. An increase in the oxide thickness, as well as the incorporation of elements (such as P, Ca, and S) from extracellular fluids into the oxide layer has been observed for long-time implantations in bone tissues by Healy and Ducheyne (1992). In fact, in vitro modelling experiments suggested that oxidation rates depend either on enzymatically generated $O_2$ and $H_2O_2$ or electric field-assisted transport of metal ions into the oxide. An eample of that is a work from Sundgren et al. (1986). Furthermore, the release of metallic ions of aluminum and vanadium, although in small amounts, may cause local irritation of the tissues surrounding the implant or, in long-term implantations (up to 20 years), the patient may become sensitized to the metallic ions released by the implant. This is nowadays well documented by several works available in the literature (e.g., Elias et al., 2008; Merritt and Rodrigo, 1996; Zitter and Plenk Jr, 1987). The accumulation of Ti and its alloying elements in tissues adjacent to the implant has been reported by several other authors, such as Schoon et al. (2020) and Wu et al. (2022). Granchi et al. (2006) reported that patients with Ti-6Al-4V hip joint or knee arthroplasty replacements had a high incidence of vanadium- positive patch testing. In addition, $Al^{3+}$ replaces $Mg^{2+}$ and $Fe^{3+}$ in patients causing disturbances associated with intercellular communication, cellular growth and secretory functions. This is critical, as the changes induced in neurons by aluminum are similar to the degenerative lesions observed in Alzheimer patients, as reported by Jaishankar et al. (2014). Abdel-Hady and Niinomi (2013) also reported metabolic-bone diseases to be caused by aluminum ions. Among these pathologies, Boyce et al. (1992) found a correlation between Al release and the insurgence of osteomalacia.

Given the possible critical insurgences related to ions release, adopting a reliable way to determine this phenomenon is mandatory. This can be measured using static immersion tests. This experimental path was adopted by Bruneel and Helsen (1988). However, the very low concentrations obtainable in reasonable times of exposure make this determination difficult. Conversely,

electrochemical tests are more convenient and commonly found in the literature. For instance, Alves et al. (2009) adopted this technique to assess the corrosion resistance of commercial purity titanium (CP Ti) and Ti-6Al-4V in a simulated body fluid at 25 °C and 37 °C. A similar methodology was used by Machado López et al. (2021) to investigate the effect of a zirconia coating on a Ti-6Al-4V substrate for orthopedical application. The electrochemical characterization is usually carried out using potentiodynamic polarization, ideal to evaluate the initiation of localized corrosion. Nevertheless, titanium is seldom affected by localized corrosion in physiological solutions. Moreover, the current values achieved in the passive range are several orders of magnitude higher than the passivity current, due to the not stationary conditions of polarization, as stated by Esmailzadeh et al. (2018). Many authors have deployed electrochemical impedance spectroscopy (EIS), which is suitable for monitoring the evolution on the passive film over time. However, due to the high electrical resistance of the titanium oxide, it is not possible to reach an asymptotic value of the impedance modulus even at very low frequencies. Hence, obtaining the charge transfer constant, thus the passivity current at equilibrium, is impossible. Given the limitations of potentiodynamic polarization and EIS techniques, a more suitable method to measure the trend of the passive current as a function of the time is to potentiostatically polarize the specimen at a potential similar to the value in human body. No other works adopting this technique to investigate LPBF-produced Ti-6Al-4V samples are currently available in the literature, at the best of the authors' knowledge. Therefore, given the current literature gap on this subject, the aim of the present work is the evaluation of the passive current density of the Ti-6Al-4V alloy produced by means of LPBF in a simulated body fluid. The samples were analyzed considering different surface finishing and heat treatments. The corrosion assessment of the alloy consisted in potentiodynamic tests at +0.500 V *vs.* SCE, which corresponds to a potential slightly higher than the one assumed for titanium alloys in the human body (Cotton and Hayfield, 1967).



## 2. Materials and Methods

### Specimens

The tests illustrated in this work were carried out on cylindrical specimens with a 15 mm diameter and 5 mm height. The LPBF-produced specimens were manufactured using an EOS M270 Dual Mode machine, equipped with a 200 W Yb fiber laser system operating in an Ar atmosphere. The main process parameters adopted were a laser power of 170 W, a scanning speed of 1250 mm/s and a hatching distance of 0.10 mm. The specimens were produced considering different orientations with respect to the building platform. The samples were built both with the base parallel to the building platform (named XY) and perpendicular to the building platform (named XZ). The feedstock gas atomized Ti-6Al-4Vpowder, supplied by EOS GmbH, was characterized by a D(10), D(50) and D(90) of 22.3, 33.4 and 47.1 µm, respectively. A traditional wrought material was also used for comparison.

The specimens manufactured via LPBF were tested in two conditions: without heat treatment (named UT specimens) and after stress relieving (named SR specimens). This process was conducted using a VF800/S Pro.Ba high-vacuum furnace, which was set to operate at 680 °C for 4 h and then slowly cool down to room temperature at approximately 1.5/2 °C/min. Throughout the heat treatment operations, the internal pressure of the instrument was always $< 10^{-5}$ mbar. The as-built specimens that did not undergo any post-processing operation are referred to as AB. To evaluate different post-processing conditions, some specimens underwent a pickling treatment with an acid mixture (25%

$HNO_3$ and 2.5% HF) for 60 seconds at room temperature (named PK). Conversely, other samples were polished (P specimens), using a 4000-grit abrasive paper and then a 1 µm diamond paste with a synthetic cloth. All these specimens were then passivated in air for one hour before testing. All the samples analyzed were degreased in acetone before corrosion testing.

### Microstructural examination

For the microstructural examination, the samples were cut, polished and chemically etched using a Kroll solution (93% $H_2O$, 5% $HNO_3$, 2% HF). Porosity evaluation by image analysis of the cross section provided a density value greater than 99.97%. Optical imaging was performed using a Leica DM ILM optical microscope, whilst SEM micrographs were acquired with a FIB-SEM Tescan S9000G microscope. Phase identification was performed using a PANalytical X-Pert Philips diffractometer in a Bragg Brentano configuration operated at 40 kV and 40 mA using a Cu Kα radiation source. A 2θ range of 30°-80° was investigated and a step size of 0.013° was considered.

### Potentiostatic tests

The potentiostatic tests were carried out in simulating body fluid solution (SBF, NaCl 8.74 g/L, $NaHCO_3$ 0.35 g/L, $Na_2HPO_4 \cdot H_2O$ 0.075 g/L, $NaH_2PO_4 \cdot H_2O$ 0.069 g/L) at 37 °C. This solution was deaerated by nitrogen bubbling for at least 1 hour before the test. A 3 electrodes cell (ASTM G5) and a PTFE sample holder with the exposed surface equal to 1 $cm^2$ were used. The specimens were polarized at +0.500 V *vs.* SCE for 60 hours whilst recording the current density. Nitrogen bubbling was performed throughout the whole duration of the measurement. The tests were repeated twice using an Ivium Compactstat potentiostat, hence two specimens per condition were tested.

Potentiostatic tests in the same conditions were performed also at longer exposure, up to 6000 hours. Eight different samples were exposed in a 25 l electrochemical cell, equipped with one reference electrode at the center and one counter electrode at the bottom. This setup was designed to grant an even current distribution over the exposed metal surfaces. The specimens were anodically polarized using a 2051 AMEL potentiostat. The data were collected using a 2000 Keithley multimeter combined with a 7001 Keithley scan system that read the ohmic drop of the shunt resistance. Due to the limited number of testable specimens, the UT specimens were not considered for long-term potentiostatic tests. This choice was made under the assumption that the LPBF-processed Ti-6Al-4V alloy is hardly ever used in this condition, due to its limited ductility, not compliant with ASTM F2924.

## 3. Results and discussion

### Characterization of the microstructures

The microstructures obtained during the identification via optical and electron microscopy are provided in Figure 1. From Figure 1a and Figure 1d it is possible to appreciate the columnar morphology of the prior-β grains in the samples in both conditions, UT and SR. This morphology is a typical outcome of the LPBF process, and it is associated with the highly directional cooling typically granted by this technology. The morphology of the prior-β grains was not altered by the stress relieving heat treatment. Higher magnification micrographs (Figure 1b,e) allowed to perform a more detailed

investigation: the samples in the as-built state were characterized by a completely α' martensitic microstructure, easily recognizable by the typical martensitic needles, placed in a ±90° fashion from each other (Carrozza et al., 2021b). Xu et al. (2015) reported that this microstructure is typical for Ti-6Al-4V when a cooling rate of at least 410 K/s is reached during the process. Conversely, the SR specimens were characterized by a more regular lamellar microstructure, induced by the α' → α+β decomposition. Notwithstanding this, the initial morphology of the α' needles in the UT samples was still recognizable in the α laths of the SR samples. SEM micrographs provide a better imaging of the α' martensite needles (Figure 1c) in the UT condition. Furthermore, the β phase developed during the heat treatment was clearly visible in the SR specimens (Figure 1f).

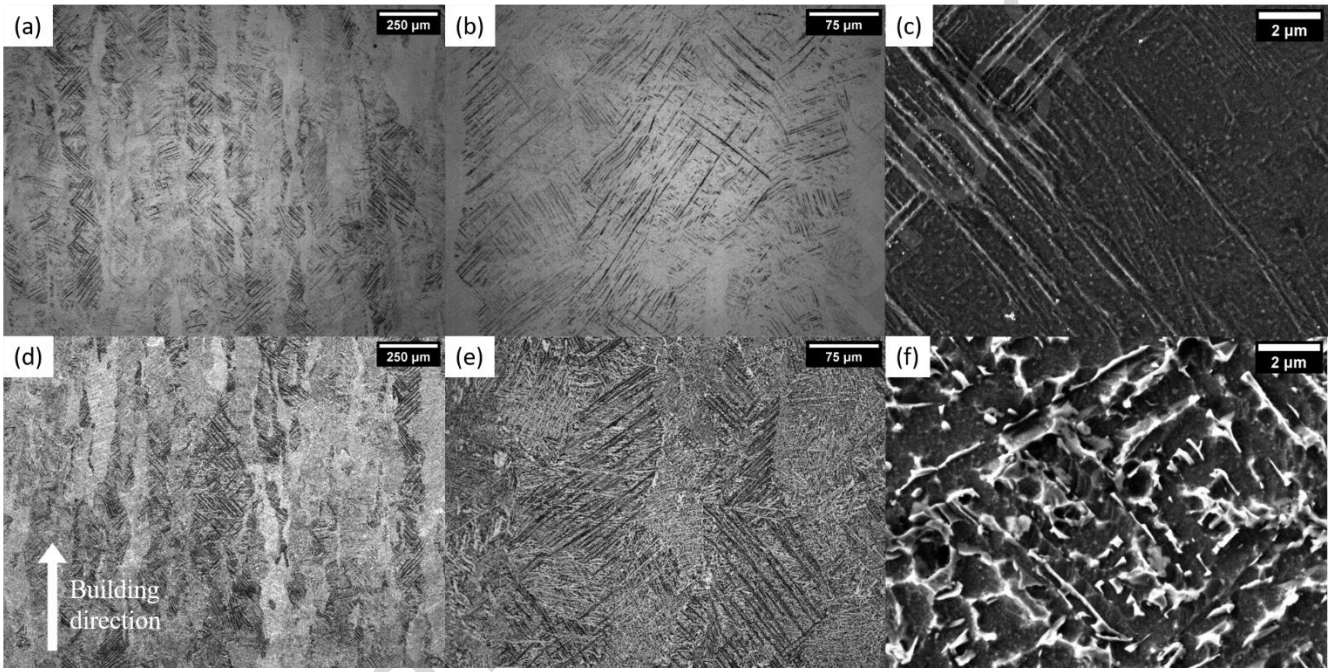


*Figure 1: Optical micrographs of the Ti-6Al-4V samples UT (a,b) and SR (d,e). SEM micrographs of the specimens in the UT (c) and SR (f) conditions.*

X-ray diffraction (XRD) analyses were performed to confirm whether the phase compositions agreed with the hypothesis about the evolution of the microstructure. The resulting diffractograms are shown in Figure 2.

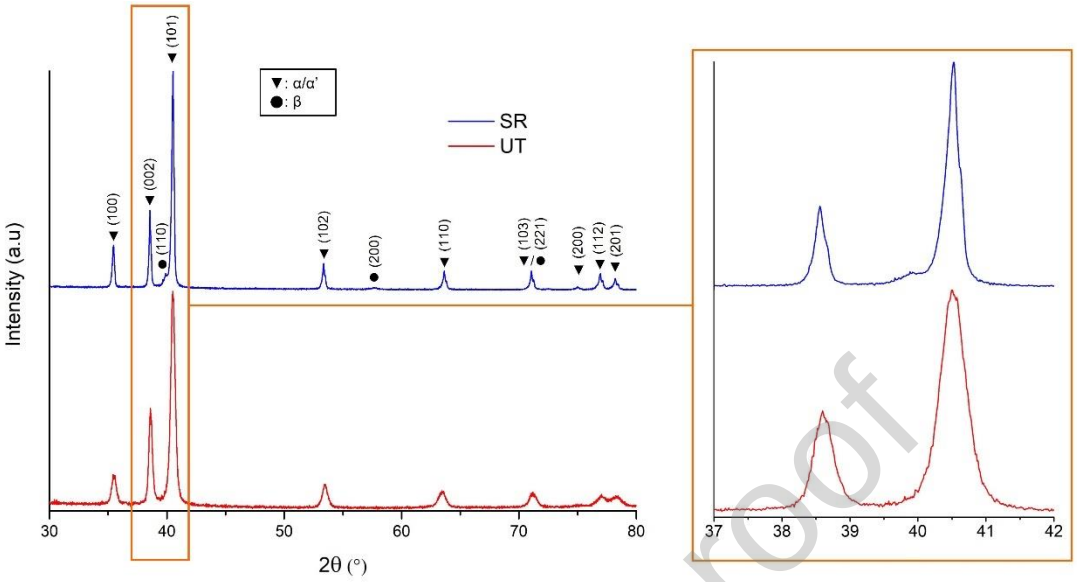


*Figure 2: XRD patterns of the samples in UT and SR conditions.*

The sample in the UT condition showed only the peaks related to the α/α' lattice (hexagonal). Considering the technology involved and its typical cooling rates, it is safe to assume that this type of samples is characterized by a 100% martensitic (α') composition (Motyka, 2021), in agreement with the result of the micrographs investigation. Conversely, the samples in the SR state were characterized by the clear presence of the (110) β-phase (bcc) peak, which is visible even if it partially overlaps with the (101) α-phase (hcp) peak. This result confirms the decomposition of the martensite during the heat treatment, shifting from the metastable α' martensite towards more thermodynamically stable phases (α+β).

**Superficial characterization**

The quality of the external surface of the specimens was strongly influenced by the building direction (Figure 3). The XY specimens provided clearly visible tracks of the laser (Figure 3a), whilst the shapes of the melt pools were recognizable in the XZ specimens. On these last surfaces the presence of many spheres was observed. This phenomenon was attributed to partially melted/unmelted and adhered particles, a typical defect for LPBF-produced samples, as discussed by Patel et al. (2020). Balling was excluded due to the presence of these defects exclusively in correspondence of the external borders of the specimens. The particles observed were not removable despite the sonication of the samples in acetone prior to the testing. The 3D surface topography reconstruction, shown in Figure 4, confirms that the roughness was significantly higher in the XZ planes. Calignano (2018) reported that the adhered particles are the main factor that determines the side roughness of LPBF-produced samples.

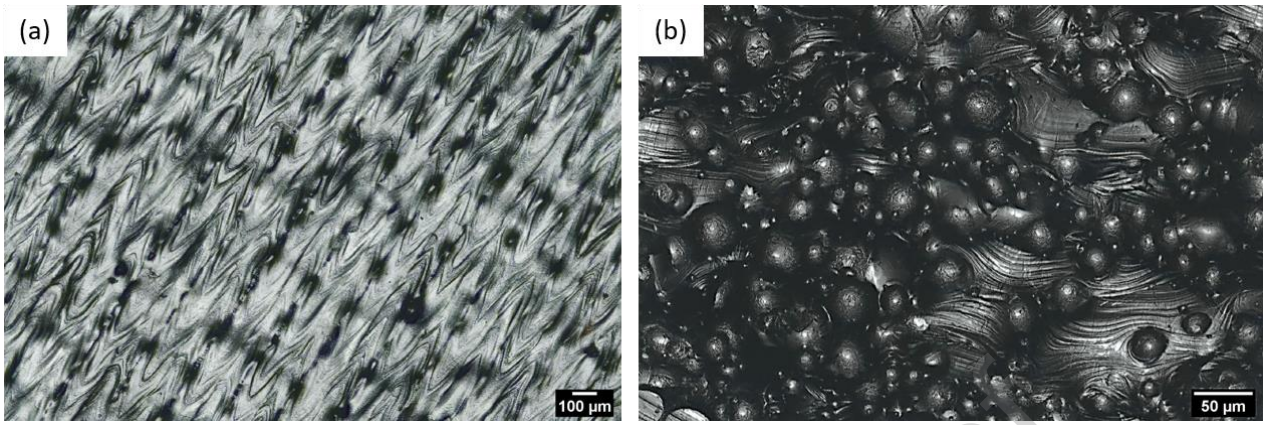


*Figure 3: Laser confocal images of LPBF-produced Ti-6Al-4V specimens from the XY (a) and XZ (b) planes.*

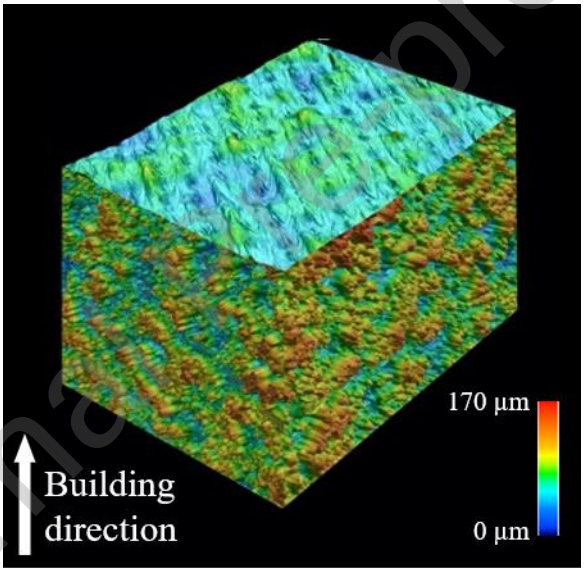


*Figure 4: 3D reconstruction of a LPBF-manufactured Ti-6Al-4V specimen.*

The lack of a strong metallurgical bonding, hence poor adherence, of the particles was confirmed by the presence of small debris that detached from the surface of the specimens after sonication at the end of the corrosion test. The release of debris is unacceptable for biomedical applications, unless a cleaning treatment (chemical and/or mechanical) is implemented. Therefore, the effect of a pickling treatment with a hydrofluoric-nitric solution on the passive current of the manufactured samples was investigated. The effect of pickling is shown in the 3D reconstruction of the XZ surface before (Figure 5a) and after 60 second of exposure in the acid solution (Figure 5b). This post-processing route resulted in a reduction of the unmelted particles and a variation of the roughness (Ra) that went from 14.5 down to 11.5 µm. However, the chemical pickling only partially removes the residual particles adhered to the surface, which are then fully removable only by means of mechanical polishing.

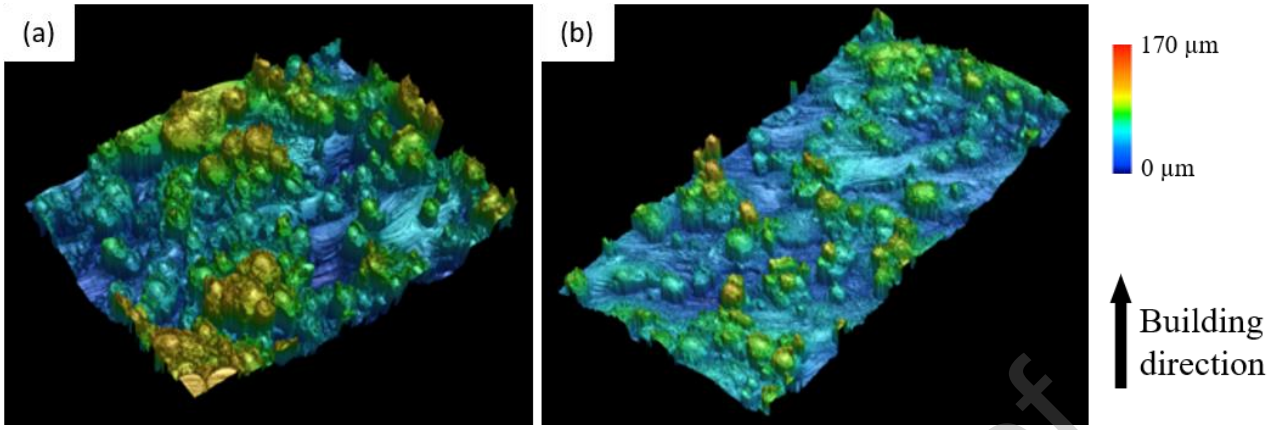


*Figure 5: Effect of the pickling treatment on the quality of the XZ LPBF surface before (a) and after (b) such procedure.*

**Potentiostatic tests**

Some examples of the potentiostatic curves obtained for LPBF-manufactured Ti-6Al-4V samples exposed in a simulated body solution at +0.500 V vs. SCE as a function of the building direction, heat treatment and superficial conditions are reported in Figure 6. These results are strictly related to the ions release rate, which is proportional to the current density developed during the test. As soon as the samples were polarized, the current density detected was very high, but decreased over exposure time. After several hours, the curves approached a steady state condition, but the stable asymptotic value was reached only after several thousands of hours of exposure. Cigada et al. (1992) found a similar behavior when characterizing the corrosion behavior of conventionally-manufactured Ti-6Al-4V in SBF.

The value $i_0$ of the current density in the first instant of polarization (

Table *1*) varied from 42 to 684 $\mu A/cm^2$ and it was not possible to identify any clear correlation between these values and the building direction, nor the heat treatment. The great data variability can be mainly attributed to the very fast passivation kinetic at early exposures, which made the exact synchronization of the measurements very complex to achieve. The AB specimens presented many spikes in the current (Figure 6). Their presence was more frequent in the XZ specimens than in the XY specimens, irrespective of the heat treatment. This behavior could be associated with the presence of unmelted particles on the surface, which were not removable, despite the sonication of the samples in acetone prior to testing (Figure 3). These particles were poorly adherent with the surface and the formation of new products, possibly due to preferential corrosion attacks, were observed at the particle/metal interface (Figure 7). Finally, the spikes were less frequent in the PK specimens, but still present. Conversely, the spikes were totally absent in the P samples, whilst the initial current values maintained the same order of magnitude (Figure 6) of the PK ones. These results confirmed the negative effect of the unmelted particles on the surfaces of the samples (Figure 4,5).

The potentiostatic tests were stopped after 60 hours of exposure. The values of the average current density in the last hours ($i_{60h}$) had a very low standard deviations, thus indicating that stationary conditions were reached (

Table *1*). These values were several orders of magnitude lower than $i_0$ - as expected - due to the continuous increase in the oxide layer thickness over exposure time.

The long-time potentiostatic tests were performed in order to experimentally evaluate the asymptotic values of the passivity current. These tests were carried out only on the PK and P specimens only, since the AB specimens could not be used in practice due to their tendency to release small debris, unacceptable in the biomedical field. Figure 8 shows the current vs. time curves relative to the potentiostatic tests with the final parts obtained from the long-time tests. The trend relative to the UT-XY-P samples is missing due to some issues experienced during the test. The average values of the current density in the last 100 hours of these last tests named $i_{6000h}$ - are reported in Table 1; these average values are characterized by a very low standard deviation and are a good indicator of the asymptotic value achieved.

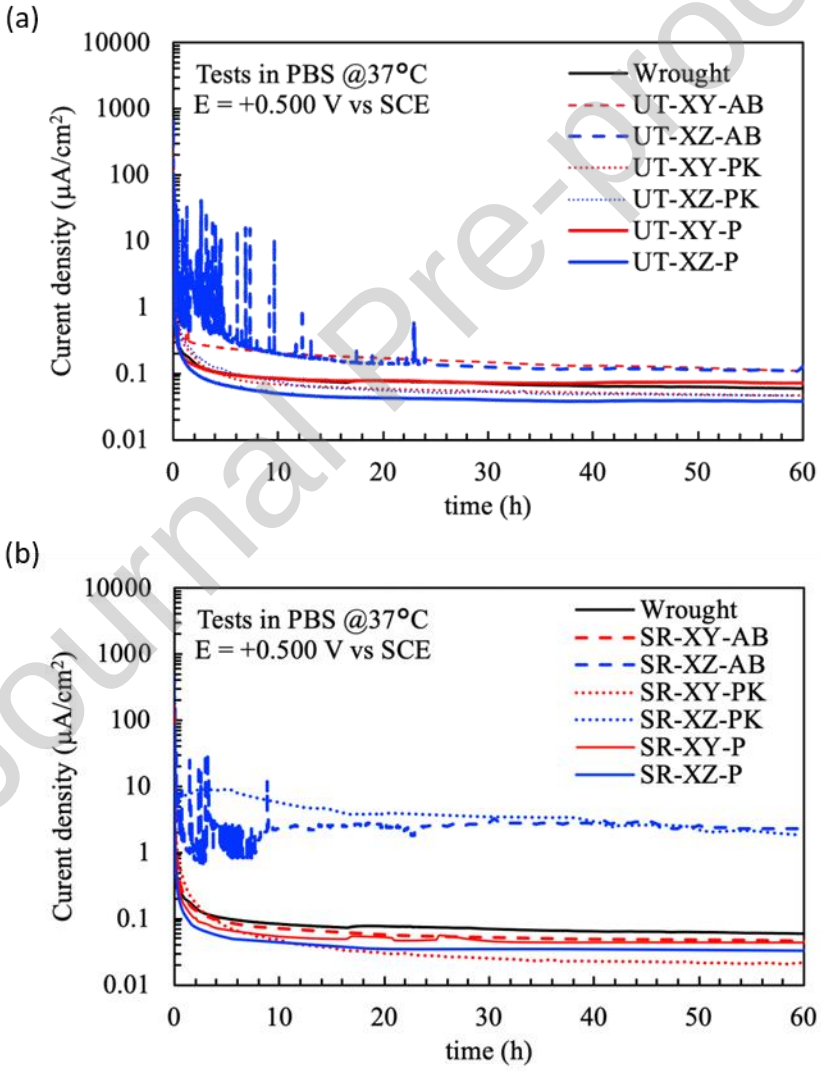


*Figure 6: Potentiostatic curves (E = +0.500 V vs SCE) for UT (a) and SR (b) samples. In both graphs the curve relative to the wought condition was used as a reference.*

*Table 1: Summary of results after short and long-time potentiostatic tests*

| *Heat treatment* | *Building direction* | *Superficial condition* | $i_0$* ($\mu A \cdot cm^{-2}$) | $i_{60h}$* ($\mu A \cdot cm^{-2}$) | $i_{6000h}$** ($\mu A \cdot cm^{-2}$) |
|---|---|---|---|---|---|
| **UT** | XY | AB | 42 | 0.111 ± 0.001 | - |
| | | | 163 | 0.042 ± 0.001 | |
| | | PK | 320 | 0.051 ± 0.003 | 0.022±0.002 |
| | | | 617 | 0.041 ± 0.002 | |
| | | P | 108 | 0.074 ± 0.001 | - |
| | | | 684 | 0.035 ± 0.002 | |
| | XZ | AB | 464 | 0.112 ± 0.0004 | - |
| | | | 463 | 0.112 ± 0.05 | |
| | | PK | 439 | 0.049 ± 0.002 | 0.032 ± 0.007 |
| | | | | | |
| | | P | 103 | 0.039 ± 0.0004 | 0.028 ± 0.002 |
| | | | 657 | 0.072 ± 0.001 | |
| **SR** | XY | AB | 51 | 0.065 ± 0.021 | - |
| | | | 43 | 0.018 ± 0.0003 | |
| | | PK | 191 | 0.060 ± 0.008 | 0.027 ± 0.002 |
| | | | 390 | 0.021 ± 0.0004 | |
| | | P | 126 | 0.049 ± 0.004 | 0.028 ± 0.002 |
| | | | 631 | 0.048 ± 0.002 | |
| | XZ | AB | 99 | 1.27 ± 0.01 | - |
| | | | 149 | 2.27 ± 0.03 | |
| | | PK | 463 | 2.06 ± 0.08 | 0.037 ± 0.002 |
| | | | 463 | 2.18 ± 0.06 | |
| | | P | 83 | 0.05 ± 0.01 | 0.048 ± 0.002 |
| | | | 314 | 0.14 ± 0.016 | |

*Average values from short time potentiostatic tests from 59 to 60 hours
**Average values from long time potentiostatic tests from 5900 to 6000 hours

The variations between the $i_{6000h}$ values of the samples in the different conditions are very low. This phenomenon indicates that, even if the initial surface conditions are significantly different, the oxide film tends to converge to a similar condition upon long immersion times. The currents of the XY specimens, independently from the superficial condition or heat-treatment, were in the range of 0.022÷0.028 μA/cm$^2$, whereas the XZ specimens were in the range of 0.028÷0.048 μA/cm$^2$. All these values are consistent with the values reported in the literature. The corrosion rate of the traditional wrought alloy (168 h immersion time) in neutral Hank's solution reported by Alves et al. (2009) is in the range of 0.030-0.164 μA/cm$^2$, De Assis et al. (2006) obtained a value of 0.019 ±0.0009 μA/cm$^2$, using a neutral Ringer solution (72 h immersion time). Vasilescu et al. (2009) reported higher values, from 0.2 to 21 μA/cm$^2$, depending on the metallurgical condition. These values were obtained by means of potentiodynamic and electrochemical impedance spectroscopy techniques and depend on the exposure time. On the contrary, long-time immersion potentiostatic tests on the same wrought alloy performed by Cigada et al. (1992) gave lower corrosion rates than the values reported above.

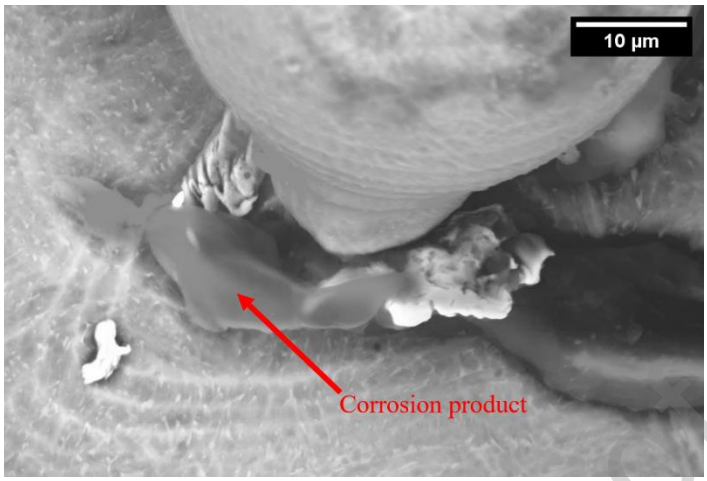


*Figure 7: SEM image of an unmelted particle on the surface of a specimen after the potentiostatic test: the presence of corrosion products highlights the lower corrosion resistance at the interface.*

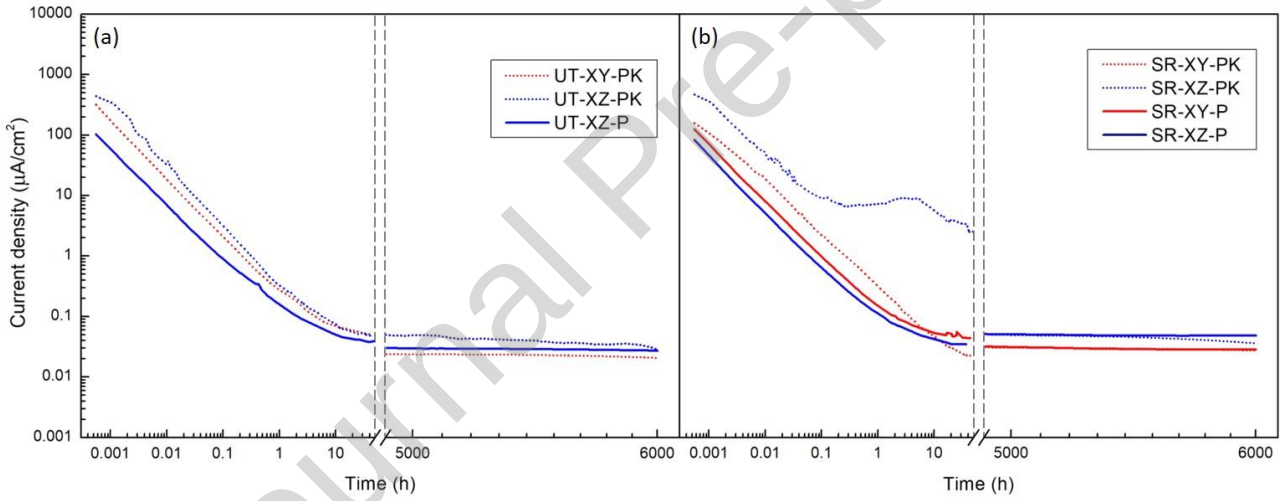


*Figure 8: Long-time potentiostatic curves at +500 mV in simulated body solution for the PK and P Ti-6Al-4V specimens.*

Some differences in the behavior of the specimens XZ specimens can be observed after 60 hours of testing (Table 1). On the contrary, the values of $i_{60h}$ of the XY specimens, are practically independent on the superficial condition or heat treatment (with the only exception of one PK sample). The effect of the post-processing heat treatment is controversial. In fact, stress relieving seemed to influence only the XZ specimens in the AB or PK conditions, generating a current density after 60 hours of exposure higher than in their non-heat-treated counterparts. Conversely, the P specimens were not affected by the heat treatment, independently upon their orientation. A decrease in corrosion resistance after heat treating the LPBF-produced samples was also found in AlSi10Mg by Cabrini et al. (2019b) and Rubben et al. (2019), Inconel 625 (Cabrini et al., 2019a) and CoCr alloy (Alifui-Segbaya et al., 2015). Conversely, a beneficial effect of the heat treatment was observed for AISI 316L and 17-4 PH steels by Chen et al. (2018) and Stoudt et al. (2017), respectively.

The post-processing polishing surface treatment helped in smoothing the high roughness of the specimens by eliminating the unmelted particles. In these conditions, the native titanium oxide formed during the LPBF process was removed, thus promoting the formation of a new oxide layer in air. This film can be considered close to the one present on the traditionally hot-worked and machined alloys. Considering that, any difference in the corrosion behavior of the P samples can be attributed exclusively to their microstructure.

The UT-P specimens showed, at the end of the short time potentiostatic test, a very slight attack, which highlighted the martensitic microstructure (Figure 9a,b). The edge of the melt pool appeared to be less resistant to corrosion, thus in these areas a selective dissolution was detected. A preferential corrosion of the melt pool borders was also detected. This was probably caused by the different microstructural features that characterized the edge, where multiple laser tracks overlapped during the process, with respect to the central part of the melt pool. In fact, tertiary/quaternary α' martensite can be found at the borders, according to the process parameters. Conversely, in the central part the martensite is usually primary, as confirmed by Dilip et al. (2017). Another possible explanation can be related the preferential corrosion to the presence of more defects at the edge of the melt pools, as reported by Agius et al. (2017). After 6000 hours of testing, the specimens appeared covered by a colored oxide layer, interrupted in some points by a shallow attack-like dendrite, starting from emerging porosities (arrows in 9c) and following the edge of the melt pools (dotted line in Figure 9c). The high corrosion resistance of the titanium alloys prevented the growth of these localized attacks, which were contained on the surface.

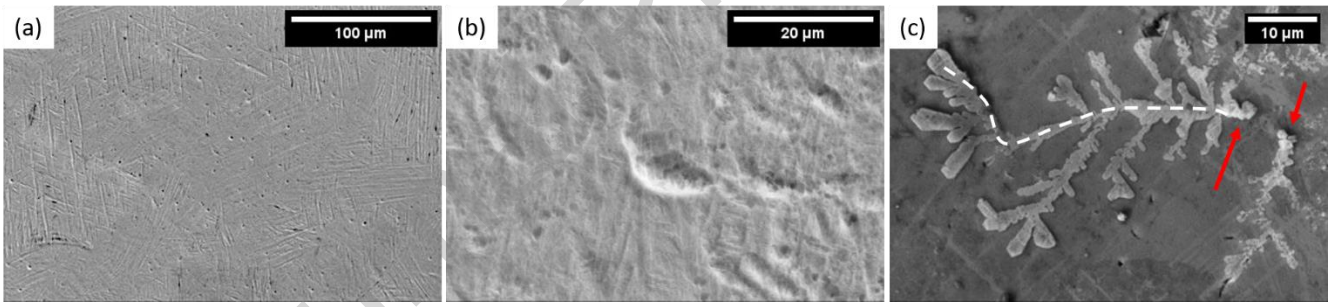


*Figure 9: SEM images of the specimens XZ-UT-P after the short-time (a,b) and long-time (c) potentiostatic tests.*

The heat treatment performed in this work led to the decomposition of the α' martensite in α and β phases, although the new lamellar microstructure inherited the preferential orientation of the α' needles in the as-built condition. Figure 10 reports the micrographs relative to the P and SR specimens after the potentiostatic tests: a light metallographic attack is evident on the specimens after the short-time tests (Figure 10a,b). This attack highlighted the presence of β phase (bright zones in Figure 10), between adjacent α lamellae, owing to the preferential dissolution of the α phase; in any case, the attack did not penetrate deep inside the specimens. After 6000 hours of potentiostatic tests, the samples were covered by a brown colored oxide. On the surface of these specimens the presence of β phase was less evident (Figure 10c), confirming the slowing of the dissolution process of the α' phase. Conversely, the passive current densities developed in this samples after 6000 hours were very similar.

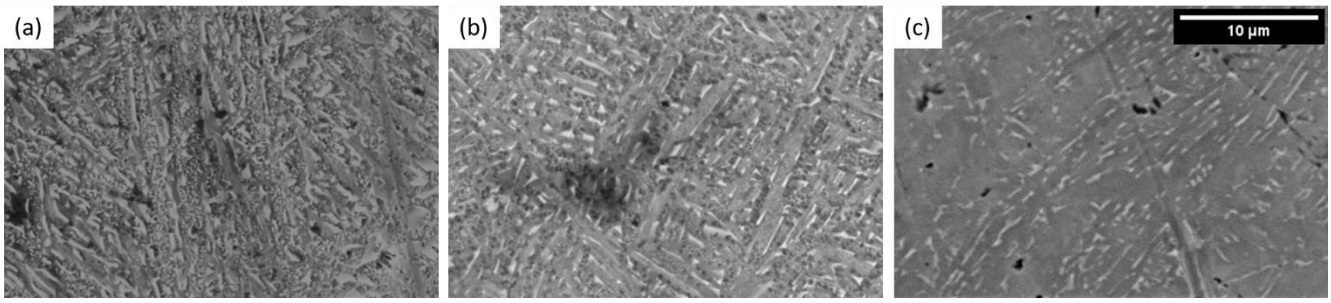


*Figure 10: SEM images of the surface of the specimen after the short time (a) XY and (b) XZ and long-time XY (c) potentiostatic tests.*

The detrimental effect of the β phase volume fraction on the corrosion resistance in 3.5 wt% NaCl of SLM-produced Ti-6Al-4V after heat treating at 500 °C, 850 °C, and 1000 °C, was reported by Dai et al. (2017) and Chandramohan et al. (2017). Conversely, Xu et al. (2017) (SBF) and Yang et al. (2017) (NaCl 3.5% solution) reported that as-printed Ti-6Al-4V part exhibited inferior corrosion resistance with respect to the commercial wrought alloy. Moreover, these authors demonstrated that a post-processing heat treatment can reduce the susceptibility of the material to corrosion. The results of these works seem to evidence a negative effect caused by the β-phase formed during the post-processing stress relieving in the LPBF-produced Ti-6Al-4V alloy. However, the SBF is definitely a mild environment for titanium-based alloys, whose corrosion resistance is expected to be quite high. Therefore, the selective dissolution of the α phase, stimulated by the presence of β-phase, is limited to the first days of exposure.

The corrosion behavior of the unpolished specimens could be attributed to the different resistance of the oxide layer formed during the laser melting and modified at high temperatures during the stress relieving. Figurer 11 compares the surface of a UT XZ specimen (UT-XZ-AB) pre-pickling (Figure 11a), post-pickling (UT- XZ-PK, Figure 11b) and after the potentiostatic test on the pickled sample (Figure 11c,d). As previously reported, the XZ specimens presented a high concentration of adhered unmelted particles and emerging defect. The pickling produced a severe corrosion of the surface of the samples. Small acidic attacks are evident on the surface, mainly located at the edge of the melt pools (arrows in Figure 11c and close-up in Figure 11d). After the potentiostatic tests, these areas were significantly enlarged. Conversely, this effect was less pronounced for the XY specimens (Figure 11e and close-up in Figure 11f). This outcome was probably due to the lower concentration of melt pool borders on the XY plane with respect to XZ.

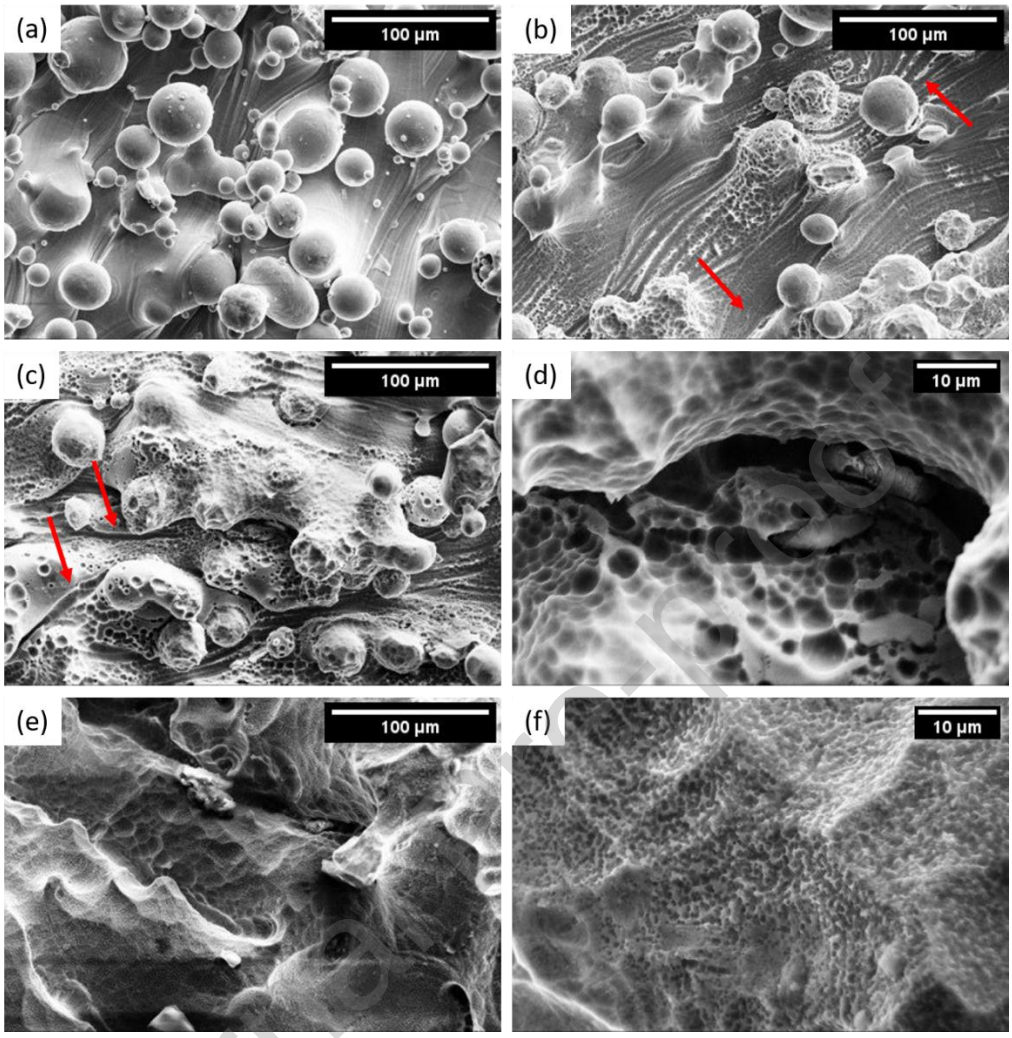


*Figure 11: SEM images of the specimens UT-XZ-AB (a), UT-XZ-PK (b), UT-XZ-PK after the potentiostatic test (c,d) and UT-XY-PK after the potentiostatic test (e,f).*

The heat treatment did not modify significantly the aspect of the surface of the as-built specimens (Figure 12a,d). However, the pickling removed most of the unmelted particles adhered on the XY specimens (Figure 12e), but not those on the XZ specimens (Figure 12b). The edge of the melt pools of the XZ samples (Figure 12b) and the areas in correspondence of the particles (Figure 7), are preferentially corroded, indicating a higher reactivity of these zones. The XY specimens only provided a shallow attack which traces of β phase (Figure 12e). After the potentiostatic test, the XY specimens were characterized by an aspect similar to that of the P specimens, with an evident lamellar microstructure with clear rods of β phase (Figure 12f). Instead, the XZ specimens showed a selective attack at the border of melt pools (Figure 12c and close-up in Figure 13).

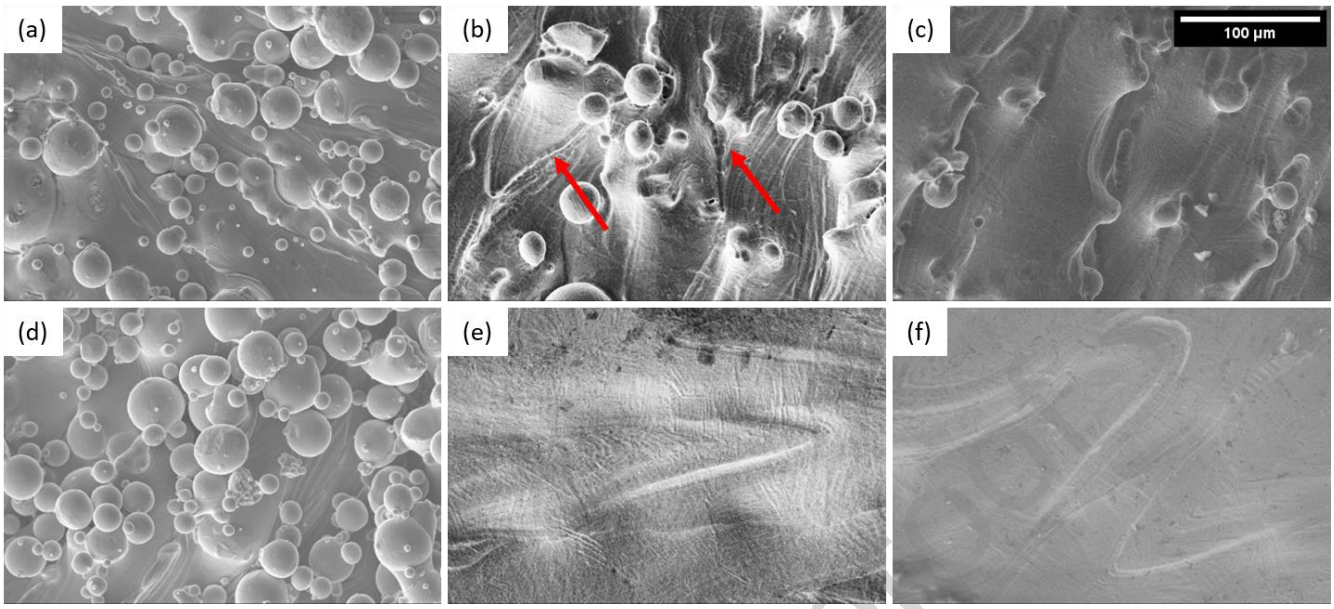


*Figure 12: SEM images of the specimens:SR-XZ-AB (a); SR-XZ-PK (b); SR-XZ-PK (c) after the potentiostatic test; SR-XY-AB (d); SR-XY-PK (e); SR-XY-PK (f) after the potentiostatic test.*

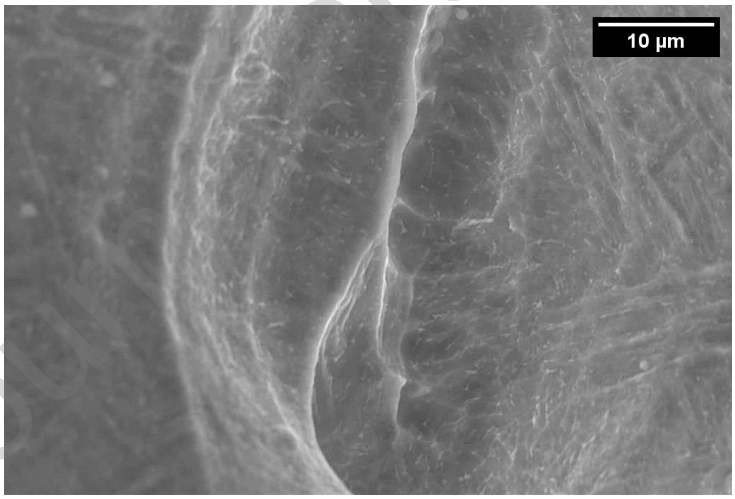


*Figure 13: Close-up of the preferential attack of the edge of the melt pool in the SR-XZ-PK specimen.*

The synergistic action of the higher concentration of unmelted particles and edges of melts pools, in conjunction with the β phase produced by the post-processing stress relieving, could explain the worst behavior observed in the XZ heat-treated specimens with respect to the XY ones. In fact, the presence of these defects is higher in the plane parallel to the building direction, than in the one parallel to the building platform. The high tendency of titanium alloys to passivate avoided the propagation of the corrosion attack inside the specimen. Moreover, this effect was limited only to the first hours of immersion. These results are consistent with the work by Chen et al. (2017) who, using different equipment and scanning strategy, observed that the samples with the exposed surface parallel to the building direction had a lower corrosion resistance than the samples with the exposed surface parallel to the building direction in Hank's solution at 37 °C. These observations were corroborated considering

that the planes parallel to the manufacturing direction had a larger number of holes and artefacts that were induced during processing with the zigzag laser scanning strategy. A worst corrosion behavior of the XZ samples with respect to XY was also observed by Dai et al. (2017) in HCl 1 M that supposed the formation of "weaker" passive layer on the planes parallel to the building direction. The building direction-dependent anisotropy in LPBF-produced Ti-6Al-4V was also observed in terms of hardness by Guzanová et al. (2017) and tensile properties by Simonelli et al. (2014).

To sum up, the present work confirms the excellent resistance to corrosion of the LPBF-produced Ti-6Al-4V alloy in SBF environment, despite the rough surfaces generated by the manufacturing process, particularly indicated to favor the growth of bone cells at the interface between the prosthesis and the diaphyseal canal (Boyan et al., 1996). However, a scanning strategy aimed to reduce the number of unmelted particles adhered to the lateral surface must be developed to reduce the formation of debris and the initial spike of current. Additionally, the pickling treatment proved to be fundamental to fully remove the unmelted particles and to allow the formation of a more protective passive film on the surface. More detailed studies to evaluate the effect of the increasing β phase fraction during the post-processing stress relieving treatment will be further performed.

## Conclusions

LPBF-produced Ti-6Al-4V samples were microstructurally and electrochemically characterized in order to investigate the effect of the manufacturing technology on the passive current, index of the ions release, in a simulating body fluid solution. The following conclusions could be drawn:

- Laser scanning confocal microscopy showed that the as-built surfaces is relevantly rough. Thus, it would be suitable for the growth of bone cells at the interface between the prosthesis and the diaphyseal canal.
- The corrosion resistance and passive current densities have been investigated using potentiostatic experiments and a correlation with the building direction for the stress-relieved specimens was found. In fact, the short-term current densities developed by the heat-treated XZ samples were orders of magnitude higher than the other samples. This is possibly related to a more sever immunological response for short time exposures.
- The LPBF-produced samples did not appear to provide any adverse effect of increase of the passive current density during long-term tests in simulated body fluid with respect to the conventionally-processed material. However, some spikes in current densities, and presumably increases in ion leaching, were detected immediately after the immersion. These spikes were associated with the unmelt powder particles adhered to the surface, formed during LPBF processing. A slight preferential attack at the edge of the melt pools was observed on the XZ specimens.
- A pickling treatment was shown to partially suppress the initial spikes of current, however longer treatments should be investigated in order to achieve a complete effectiveness.

## References


Abdel-Hady Gepreel, M., Niinomi, M., 2013. Biocompatibility of Ti-alloys for long-term implantation. Journal of the Mechanical Behavior of Biomedical Materials 20, 407–415. https://doi.org/10.1016/J.JMBBM.2012.11.014

Agius, D., Kourousis, K.I., Wallbrink, C., Song, T., 2017. Cyclic plasticity and microstructure of as-built SLM Ti-6Al-4V: The effect of build orientation. Materials Science and Engineering: A 701, 85–100. https://doi.org/10.1016/J.MSEA.2017.06.069

Alifui-Segbaya, F., Lewis, J., Eggbeer, D., Williams, R.J., 2015. In vitro corrosion analyses of heat treated cobalt-chromium alloys manufactured by direct metal laser sintering. Rapid Prototyping Journal. https://doi.org/10.1108/RPJ-11-2012-0110

Alves, V.A., Reis, R.Q., Santos, I.C.B., Souza, D.G., de, T., Pereira-da-Silva, M.A., Rossi, A., da Silva, L.A., 2009. In situ impedance spectroscopy study of the electrochemical corrosion of Ti and Ti-6Al-4V in simulated body fluid at 25 °C and 37 °C. Corrosion Science. https://doi.org/10.1016/j.corsci.2009.06.035

Arabnejad, S., Burnett Johnston, R., Pura, J.A., Singh, B., Tanzer, M., Pasini, D., 2016. High-strength porous biomaterials for bone replacement: A strategy to assess the interplay between cell morphology, mechanical properties, bone ingrowth and manufacturing constraints. Acta Biomaterialia 30, 345–356. https://doi.org/10.1016/j.actbio.2015.10.048

Aufa, A.N., Hassan, M.Z., Ismail, Z., 2022. Recent advances in Ti-6Al-4V additively manufactured by selective laser melting for biomedical implants: Prospect development. Journal of Alloys and Compounds 896, 163072.

Bertol, L.S., Júnior, W.K., Silva, F.P. da, Aumund-Kopp, C., 2010. Medical design: Direct metal laser sintering of Ti-6Al-4V. Materials and Design 31, 3982–3988. https://doi.org/10.1016/j.matdes.2010.02.050

Boyan, B.D., Hummert, T.W., Dean, D.D., Schwartz, Z., 1996. Role of material surfaces in regulating bone and cartilage cell response. Biomaterials 17, 137–146. https://doi.org/10.1016/0142-9612(96)85758-9

Boyce, B.F., Byars, J., McWilliams, S., Mocan, M.Z., Elder, H.Y., Boyle, I.T., Junor, B.J., 1992. Histological and electron microprobe studies of mineralisation in aluminium-related osteomalacia. Journal of Clinical Pathology 45, 502–508. https://doi.org/10.1136/JCP.45.6.502

Bruneel, N., Helsen, J.A., 1988. In vitro simulation of biocompatibility of Ti-Al-V. Journal of Biomedical Materials Research 22, 203–214. https://doi.org/10.1002/JBM.820220305

Buchanan, R.A., Rigney Jr, E.D., Williams, J.M., 1987. Ion implantation of surgical Ti- 6Al- 4V for improved resistance to wear- accelerated corrosion. J Biomed Mater Res 21, 355–366.

Cabrini, M., Lorenzi, S., Testa, C., Pastore, T., Brevi, F., Biamino, S., Fino, P., Manfredi, D., Marchese, G., Calignano, F., Scenini, F., 2019a. Evaluation of Corrosion Resistance of Alloy 625 Obtained by Laser Powder Bed Fusion. Journal of The Electrochemical Society 166, C3399–C3408. https://doi.org/10.1149/2.0471911jes

Cabrini, M., Lorenzi, S., Testa, C., Pastore, T., Manfredi, D., Lorusso, M., Calignano, F., Fino, P., 2019b. Statistical approach for electrochemical evaluation of the effect of heat treatments on the corrosion resistance of AlSi10Mg alloy by laser powder bed fusion. Electrochimica Acta 305, 459–466. https://doi.org/10.1016/j.electacta.2019.03.103

Calignano, F., 2018. Investigation of the accuracy and roughness in the laser powder bed fusion process. Virtual and Physical Prototyping 13, 97–104.

Carrozza, A., Aversa, A., Fino, P., Lombardi, M., 2021a. A study on the microstructure and mechanical properties of the Ti-6Al-2Sn-4Zr-6Mo alloy produced via Laser Powder Bed Fusion. Journal of Alloys and Compounds 870. https://doi.org/10.1016/j.jallcom.2021.159329

Carrozza, A., Mazzucato, F., Aversa, A., Lombardi, M., Bondioli, F., Biamino, S., Valente, A., Fino, P., 2021b. Single Scans of Ti-6Al-4V by Directed Energy Deposition: A Cost and Time Effective Methodology to Assess the Proper Process Window. Metals and Materials International 27. https://doi.org/10.1007/s12540-020-00930-3

Chandramohan, P., Bhero, S., Obadele, B.A., Olubambi, P.A., 2017. Laser additive manufactured Ti–6Al–4V alloy: tribology and corrosion studies. International Journal of Advanced Manufacturing Technology. https://doi.org/10.1007/s00170-017-0410-2

Chen, L.Y., Huang, J.C., Lin, C.H., Pan, C.T., Chen, S.Y., Yang, T.L., Lin, D.Y., Lin, H.K., Jang, J.S.C., 2017. Anisotropic response of Ti-6Al-4V alloy fabricated by 3D printing selective laser melting. Materials Science and Engineering A 682, 389–395. https://doi.org/10.1016/j.msea.2016.11.061

Chen, Q., Thouas, G.A., 2015. Metallic implant biomaterials. Materials Science and Engineering: R: Reports 87, 1–57. https://doi.org/10.1016/J.MSER.2014.10.001

Chen, X., Li, J., Cheng, X., Wang, H., Huang, Z., 2018. Effect of heat treatment on microstructure, mechanical and corrosion properties of austenitic stainless steel 316L using arc additive manufacturing. Materials Science and Engineering: A 715, 307–314.

Cigada, A., Cabrini, M., Pedeferri, P., 1992. Increasing of the corrosion resistance of the Ti6Al4V alloy by high thickness anodic oxidation. Journal of Materials Science: Materials in Medicine. https://doi.org/10.1007/BF00701236

Cotton, J.B., Hayfield, P.C.S., 1967. Decorative finishes on titanium. Transactions of the IMF 45, 48–52.

Cruz, N., Gil, J., Punset, M., Manero, J.M., Tondela, J.P., Verdeguer, P., Aparicio, C., Rúperez, E., 2022. Relevant aspects of piranha passivation in Ti6Al4V alloy dental meshes. Coatings 12, 154.

Dai, N., Zhang, J., Chen, Y., Zhang, L.-C., 2017. Heat Treatment Degrading the Corrosion Resistance of Selective Laser Melted Ti-6Al-4V Alloy. Journal of The Electrochemical Society 164, C428. https://doi.org/10.1149/2.1481707JES

Dai, N., Zhang, L.-C., Zhang, J., Chen, Q., Wu, M., 2016. Corrosion behavior of selective laser melted Ti-6Al-4 V alloy in NaCl solution. Corrosion Science 102, 484–489.

De Assis, S.L., Wolynec, S., Costa, I., 2006. Corrosion characterization of titanium alloys by electrochemical techniques, in: Electrochimica Acta. https://doi.org/10.1016/j.electacta.2005.02.121

Dilip, J.J.S., Zhang, S., Teng, C., Zeng, K., Robinson, C., Pal, D., Stucker, B., 2017. Influence of processing parameters on the evolution of melt pool, porosity, and microstructures in Ti-6Al-4V alloy parts fabricated by selective laser melting. Progress in Additive Manufacturing 2, 157–167. https://doi.org/10.1007/s40964-017-0030-2

Elias, C.N., Lima, J.H.C., Valiev, R., Meyers, M.A., 2008. Biomedical applications of titanium and its alloys. Jom 60, 46–49.

Esmailzadeh, S., Aliofkhazraei, M., Sarlak, H., 2018. Interpretation of cyclic potentiodynamic polarization test results for study of corrosion behavior of metals: A review. Protection of metals and physical chemistry of surfaces 54, 976–989.

Fojt, J., Fousova, M., Jablonska, E., Joska, L., Hybasek, V., Pruchova, E., Vojtech, D., Ruml, T., 2018. Corrosion behaviour and cell interaction of Ti-6Al-4V alloy prepared by two techniques of 3D printing. Materials Science and Engineering: C 93, 911–920. https://doi.org/10.1016/J.MSEC.2018.08.066

Frazier, W.E., 2014. Metal additive manufacturing: A review. Journal of Materials Engineering and Performance 23, 1917–1928. https://doi.org/10.1007/s11665-014-0958-z

Granchi, D., Cenni, E., Tigani, D., Trisolino, G., Baldini, N., Giunti, A., 2008. Sensitivity to implant materials in patients with total knee arthroplasties. Biomaterials 29, 1494–1500. https://doi.org/10.1016/J.BIOMATERIALS.2007.11.038

Groessner-Schreiber, B., Tuan, R., 1992. Enhanced extracellular matrix production and mineralization by osteoblasts cultured on titanium surfaces in vitro. undefined.

Guo, S., Lu, Y., Wu, S., Liu, L., He, M., Zhao, C., Gan, Y., Lin, Junjie, Luo, J., Xu, X., Lin, Jinxin, 2017. Preliminary study on the corrosion resistance, antibacterial activity and cytotoxicity of selective-laser-melted Ti6Al4V-xCu alloys. Materials Science and Engineering: C 72, 631–640. https://doi.org/https://doi.org/10.1016/j.msec.2016.11.126

Guzanová, A., Ižaríková, G., Brezinová, J., Živčák, J., Draganovská, D., Hudák, R., 2017. Influence of build orientation, heat treatment, and laser power on the hardness of Ti6Al4V manufactured using the DMLS process. Metals (Basel). https://doi.org/10.3390/met7080318

Healy, K.E., Ducheyne, P., 1992. Hydration and preferential molecular adsorption on titanium in vitro. Biomaterials 13, 553–561. https://doi.org/10.1016/0142-9612(92)90108-Z

Jaishankar, M., Tseten, T., Anbalagan, N., Mathew, B.B., Beeregowda, K.N., 2014. Toxicity, mechanism and health effects of some heavy metals. Interdisciplinary Toxicology 7, 60. https://doi.org/10.2478/INTOX-2014-0009

Kaur, S., Ghadirinejad, K., H. Oskouei, R., 2019. An overview on the tribological performance of titanium alloys with surface modifications for biomedical applications. Lubricants 7, 65.

Kienapfel, H., Sprey, C., Wilke, A., Griss, P., 1999. Implant fixation by bone ingrowth. The Journal of Arthroplasty 14, 355–368. https://doi.org/https://doi.org/10.1016/S0883-5403(99)90063-3

Kolli, R.P., Devaraj, A., 2018. A review of metastable beta titanium alloys. Metals (Basel) 8, 1–41. https://doi.org/10.3390/met8070506

Liu, S., Shin, Y.C., 2018. Additive manufacturing of Ti6Al4V alloy: A review. Materials & Design 164, 8–12. https://doi.org/10.1016/j.matdes.2018.107552

Liu, W., Liu, S., Wang, L., 2019. Surface modification of biomedical titanium alloy: micromorphology, microstructure evolution and biomedical applications. Coatings 9, 249.

Longhitano, G.A., Arenas, M.A., Conde, A., Larosa, M.A., Jardini, A.L., Zavaglia, C.A. de C., Damborenea, J.J., 2018. Heat treatments effects on functionalization and corrosion behavior of Ti-6Al-4V ELI alloy made by additive manufacturing. Journal of Alloys and Compounds 765, 961–968. https://doi.org/10.1016/J.JALLCOM.2018.06.319

Machado López, M.M., Calderón, F.R., Hernández, H.J., Villalobos, J.C., García, M.E., 2021. Structural and Electrochemical Characterization of the Zirconia Coating on the Ti6Al4V Alloy in Physiological Solution for Orthopedic Applications. Protection of Metals and Physical Chemistry of Surfaces 57, 1251–1261.

Merritt, K., Rodrigo, J.J., 1996. Immune response to synthetic materials: sensitization of patients receiving orthopaedic implants. Clinical Orthopaedics and Related Research (1976-2007) 326, 71–79.

Motyka, M., 2021. Martensite Formation and Decomposition during Traditional and AM Processing of Two-Phase Titanium Alloys—An Overview. Metals (Basel) 11, 481.

Okazaki, Y., Gotoh, E., 2005. Comparison of metal release from various metallic biomaterials in vitro. Biomaterials 26, 11–21. https://doi.org/10.1016/J.BIOMATERIALS.2004.02.005

Pal, S., Finšgar, M., Bončina, T., Lojen, G., Brajlih, T., Drstvenšek, I., 2021. Effect of surface powder particles and morphologies on corrosion of Ti-6Al-4 V fabricated with different energy densities in selective laser melting. Materials & Design 211, 110184.

Patel, S., Rogalsky, A., Vlasea, M., 2020. Towards understanding side-skin surface characteristics in laser powder bed fusion. Journal of Materials Research 35, 2055–2064.

Pathania, A., Subramaniyan, A.K., Nagesha, B.K., 2022. Influence of post-heat treatments on microstructural and mechanical properties of LPBF-processed Ti6Al4V alloy. Progress in Additive Manufacturing 1–21.

Rubben, T., Revilla, R.I., De Graeve, I., 2019. Influence of heat treatments on the corrosion mechanism of additive manufactured AlSi10Mg. Corrosion Science 147, 406–415. https://doi.org/10.1016/j.corsci.2018.11.038

Schoon, J., Hesse, B., Rakow, A., Ort, M.J., Lagrange, A., Jacobi, D., Winter, A., Huesker, K., Reinke, S., Cotte, M., 2020. Metal- Specific Biomaterial Accumulation in Human Peri- Implant Bone and Bone Marrow. Advanced Science 7, 2000412.

Sharma, A., Oh, M.C., Kim, J.-T., Srivastava, A.K., Ahn, B., 2020. Investigation of electrochemical corrosion behavior of additive manufactured Ti–6Al–4V alloy for medical implants in different electrolytes. Journal of Alloys and Compounds 830, 154620.

Simonelli, M., Tse, Y.Y., Tuck, C., 2014. Effect of the build orientation on the mechanical properties and fracture modes of SLM Ti–6Al–4V. Materials Science and Engineering: A 616, 1–11. https://doi.org/https://doi.org/10.1016/j.msea.2014.07.086

Stoudt, M.R., Ricker, R.E., Lass, E.A., Levine, L.E., 2017. Influence of Postbuild Microstructure on the Electrochemical Behavior of Additively Manufactured 17-4 PH Stainless Steel. JOM. https://doi.org/10.1007/s11837-016-2237-y

Sundgren, J.E., Bodö, P., Lundström, I., 1986. Auger electron spectroscopic studies of the interface between human tissue and implants of titanium and stainless steel. Journal of Colloid and Interface Science 110, 9–20. https://doi.org/10.1016/0021-9797(86)90348-6

Trevisan, F., Calignano, F., Aversa, A., Marchese, G., Lombardi, M., Biamino, S., Ugues, D., Manfredi, D., 2018. Additive manufacturing of titanium alloys in the biomedical field: processes, properties and applications. J Appl Biomater Funct Mater 16, 57–67.

Vasilescu, E., Drob, P., Raducanu, D., Cinca, I., Mareci, D., Calderon Moreno, J.M., Popa, M., Vasilescu, C., Mirza Rosca, J.C., 2009. Effect of thermo-mechanical processing on the corrosion resistance of Ti6Al4V alloys in biofluids. Corrosion Science. https://doi.org/10.1016/j.corsci.2009.08.014

Wu, J., Li, M., Lin, C., Gao, P., Zhang, R., Li, X., Zhang, J., Cai, K., 2022. Moderated crevice corrosion susceptibility of Ti6Al4V implant material due to albumin-corrosion interaction. Journal of Materials Science & Technology 109, 209–220.

Xu, W., Brandt, M., Sun, S., Elambasseril, J., Liu, Q., Latham, K., Xia, K., Qian, M., 2015. Additive manufacturing of strong and ductile Ti–6Al–4V by selective laser melting via in situ martensite decomposition. Acta Materialia 85, 74–84. https://doi.org/10.1016/J.ACTAMAT.2014.11.028

Xu, Y., Lu, Y., Sundberg, K.L., Liang, J., Sisson, R.D., 2017. Effect of Annealing Treatments on the Microstructure, Mechanical Properties and Corrosion Behavior of Direct Metal Laser Sintered Ti-6Al-4V. Journal of Materials Engineering and Performance 26, 2572–2582. https://doi.org/10.1007/s11665-017-2710-y

Yan, X., Shi, C., Liu, T., Ye, Y., Chang, C., Ma, W., Deng, C., Yin, S., Liao, H., Liu, M., 2020. Effect of heat treatment on the corrosion resistance behavior of selective laser melted Ti6Al4V ELI. Surface and Coatings Technology 396, 125955.

Yang, J., Yang, H., Yu, H., Wang, Z., Zeng, X., 2017b. Corrosion Behavior of Additive Manufactured Ti-6Al-4V Alloy in NaCl Solution. Metallurgical and Materials Transactions A: Physical Metallurgy and Materials Science. https://doi.org/10.1007/s11661-017-4087-9

Zitter, H., Plenk Jr, H., 1987. The electrochemical behavior of metallic implant materials as an indicator of their biocompatibility. J Biomed Mater Res 21, 881–896.

# CRediT author statement

**Cabrini Marina**: Conceptualization; Methodology; Resources; Writing – Original Draft; Writing – Review & Editing; Supervision.
**Carrozza Alessandro**: Conceptualization; Methodology; Validation; Formal Analysis; Investigation; Data Curation; Writing – Original Draft; Visualization.
**Lorenzi Sergio**: Conceptualization; Methodology; Investigation; Resources; Writing – Original Draft; Writing – Review & Editing; Supervision.
**Pastore Tommaso**: Writing – Review & Editing; Supervision; Project Administration; Funding acquisition.
**Testa Cristian**: Conceptualization; Validation; Investigation; Data Curation; Visualization.
**Manfredi Diego**: Formal Analysis; Supervision.
**Fino Paolo**: Project Administration; Funding Acquisition.
**Scenini Fabio**: Investigation; Visualization; Supervision.

**Declaration of interests**

☒ The authors declare that they have no known competing financial interests or personal relationships that could have appeared to influence the work reported in this paper.